Inorganic Chemistry

pubs.acs.org/IC Article

Synthetic Approaches to Metallo-Supramolecular Co^{II} Polygons and Potential Use for H_2O Oxidation

Ayuk M. Ako,[⊥] Amal Cherian Kathalikkattil,[⊥] Rory Elliott,[⊥] Joaquín Soriano-López,[⊥] Ian M. McKeogh, Muhammad Zubair, Nianyong Zhu, Max García-Melchor, Paul E. Kruger, and Wolfgang Schmitt*

Cite This: https://dx.doi.org/10.1021/acs.inorgchem.0c02182 Read Online

ACCESS | Metrics & More | Article Recommendations | Supporting Information

ABSTRACT: Metal-directed self-assembly has been applied to prepare supramolecular coordination polygons which adopt tetrahedral (**1**) or trigonal disklike topologies (**2**). In the solid state, **2** assembles into a stable halide−metal−organic material (**Hal-MOM-2**), which catalyzes H_2O oxidation under photo- and electrocatalytic conditions, operating with a maximum TON = 78 and TOF = 1.26 s^{-1}. DFT calculations attribute the activity to a Co^{III}-oxyl species. This study provides the first account of how Co^{II} imine based supramolecules can be employed as H_2O oxidation catalysts.

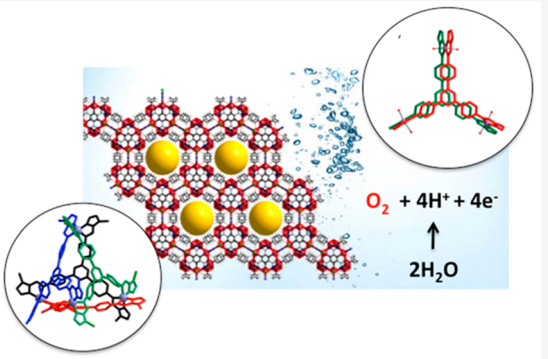

INTRODUCTION

Coordination cages and polygons represent metallo-supramolecular species in which metal ions, or small polynuclear complexes, are linked through organic ligands to produce molecular entities with well-defined geometries and cavities.[1−3] Over the last decades, research has focused on the preparation of topologies whose structural, constitutional, and electronic attributes affect catalysis,[4,5] drug delivery,[6] sensing,[7] and other areas of interest.[8−13] Directed syntheses often employ adaptions of "reticular" synthesis concepts using carboxylate-,[14,15] pyridine-, catecholate-, or imine-based ligands.[1−3,16−26] Tetrahedral M_4L_6 and M_4L_4 cages are remarkable,[16−19,24−26] some of which exemplify enzymatic reaction characteristics.[4,5] Cages containing pseudo-C_3-symmetric tris-bidentate-imine moieties include face-capped M_4L_4 tetrahedral cages that often incorporate Zn^{II} and Fe^{II} metal ions.[16−19,24−26] Although it is well understood that the nature of the metal ion strongly influences the physicochemical characteristics of imine-based cage systems,[16−19,24−26] surprisingly, the corresponding Co^{II}-based assemblies remain relatively unexplored, whereby structural data on tetrahedral face-capped $Co^{II}{}_4L_4$ species have yet to be reported.

To establish new supramolecular Co^{II} catalysts, our efforts were directed toward the synthesis of {Co^{II}/imine} species with partially hydrated coordination environments that facilitate substrate binding and organo-catalytic oxidations[4] or H_2O oxidation. The latter is motivated by the necessity to develop sustainable, carbon-neutral energy concepts.[27] Owing to its abundance, H_2O represents an obvious source of reducing equivalents to produce H_2—thus enabling the storage of solar energy in energy-dense chemical bonds. However, breakthroughs are hampered by the lack of efficient and cost-effective catalysts for the highly endergonic H_2O oxidation half-reaction.[27,28] To date, mainly noble-metal oxides (or related molecular species) provide stable catalysts with satisfactory O_2 conversion rates.[29,30] In recent years, new catalysts containing earth-abundant metal ions have beenemerging.[31−37] Molecular species are noteworthy, containing Co^{II},[31,32] Cu^{II},[31,33] and Fe^{II} or Ni^{II} ions,[31,34−37] whose coordination environments are commensurable to those of imine-based complexes.[31]

Herein a new class of heterogeneous, molecule-based H_2O oxidation catalysts is reported. The synthetic methodology involves Co^{II}-directed self-assembly using *N*,*N*′,*N*″-tris(1-methyl-1*H*-imidazol-2-ylmethylene)-1,3,5-triphenylbenzene (**L1**) and *N*,*N*′,*N*″-tris(1*H*-imidazol-4-ylmethylene)-1,3,5-triphenyl benzene (**L2**) to form tetrahedral $[Co^{II}{}_4(\mathbf{L1})_4]^{8+}$ (**1**) and disklike $[Co^{II}{}_3(\mathbf{L2})_2(H_2O)_6]^{6+}$ (**2**) supramolecules. In the solid state, **2** assembles through Cl^-−CH interactions into a stable, water-insoluble halide−metal−organic material (**Hal-MOM-2**) with large solvent-accessible voids. **Hal-MOM-2** promotes light-driven and electrocatalytic H_2O oxidation;

Received: July 27, 2020

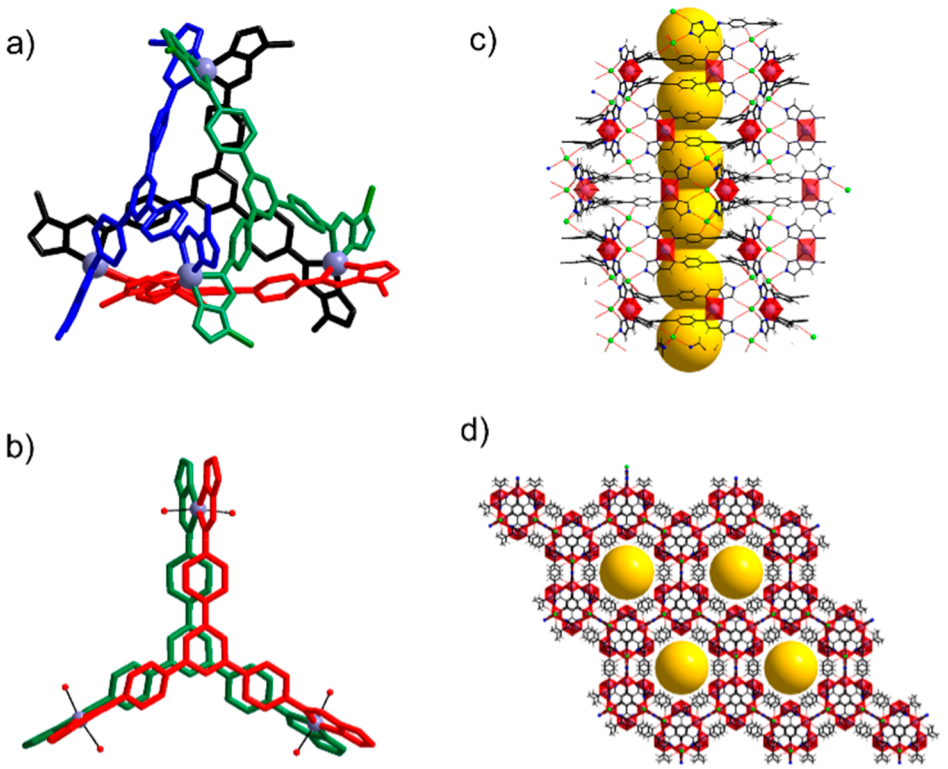

Figure 1. (a) Crystal structure of $[Co^{II}_4(\mathbf{L1})_4]^{8+}$ (**1**). (b) Structure of $Co^{II}_3(\mathbf{L2})_2(H_2O)_6]^{6+}$ (**2**) (H atoms omitted for clarity). (c, d) Views of the 3D structure of **Hal-MOM-2** in the directions of the crystallographic *a* and *c* axes, respectively. Color code: Co^{II}, red polyhedra; C, gray; N, blue; Cl, green; H, white. Yellow spheres highlight the void space.

Scheme 1. Representation of the Formation of the Tetra- and Trinuclear Species in Solution[a]

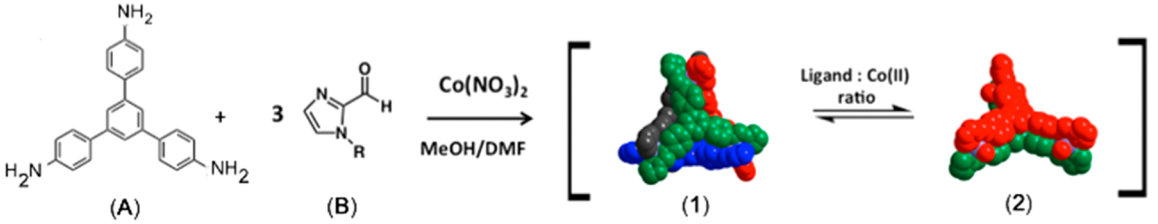

[a]R = Me (**L1**).

DFT studies elucidate the mechanism and attribute activity to a Co^{III}-oxyl species.

RESULTS AND DISCUSSION

Initial UV−vis titrations in DMF using 1,3,5-tri(4-aminophenyl)benzene (**A**), 1-methyl-2-imidazolecarboxaldehyde (**B**), and $Co(NO_3)_2 \cdot 6H_2O$ confirm the *in situ* synthesis of **L1** and the formation of Co^{II} complexes in solution (Figure 1 and Scheme 1; also see the Supporting Information). Depending on the relative reactant concentrations, $\{Co_4\mathbf{L1}_4\}$ and $\{Co_3\mathbf{L1}_2\}$ species are identifiable using ESI-MS (Supporting Information). Consequent optimization of the reaction conditions and the use of either **L1** or **L2** resulted in the crystallization of $[Co^{II}_4\mathbf{L1}_4]^{8+}$ (**1**) and $[Co^{II}_3\mathbf{L2}_2(H_2O)_6]^{6+}$ (**2**), respectively. **1** is a tetranuclear complex in which the four Co^{II} ions are located on the vertices of a tetrahedral topology (Figure 1a). Each Co^{II} ion is chelated by three imine-imidazole moieties that are derived from three different **L1** ligands, resulting in an octahedral $\{N_6\}$ coordination geometry. Altogether, the structure is stabilized by four **L1** ligands, giving rise to a *T*-symmetric, face-capped tetrahedral cage whose symmetry is characterized by four 3-fold and three 2-fold axes. The Co^{II}−Co^{II} distances are ca. 14.58 Å, while the Co−N bond lengths are 2.0564(5) and 2.1841(5) Å. Thus, **1** is related to reported Zn^{II} and Fe^{II} cages.[16−19,24−26]

Hal-MOM-2 crystallizes in the hexagonal space group $P6_122$. It contains the trinuclear, trigonal-disklike complex $[Co_3(\mathbf{L2})_2(H_2O)_6]^{6+}$ in which the Co^{II} centers are coordinated by two **L2** ligands whose aromatic ring systems align parallel to each other and are stabilized by $\pi-\pi$ interactions (Figure 1b). The Co^{II} centers in **2** display distorted-octahedral coordination geometries. The imine-imidazole moieties act as *cis*-coordinating bidentate functionalities, and their N-donor atoms are located in the equatorial plane. H_2O ligands occupy the remaining apical Co^{II} coordination sites. The packing of $[Co_3(\mathbf{L2})_2(H_2O)_6]^{6+}$ molecules generates a hexagonal assembly via H bonds, involving coordinated H_2O and constitutional solvent molecules. The complexes are further connected through interactions between Cl^- counterions and H atoms of **L2** to form the extended halide−metal−organic material **Hal-MOM-2**. The $Cl^-\cdots H_{imidazole}$ interactions occur over

https://dx.doi.org/10.1021/acs.inorgchem.0c02182
Inorg. Chem. XXXX, XXX, XXX−XXX

distances of ca. 2.19−2.29 Å. On consideration of interatomic N···Cl^- distances varying between 3.07 and 3.17 Å, these interactions can be classified as moderately strong.[38,39] The formation of a highly interconnected network involving various such supramolecular interactions is expected to contribute significantly to the stability of the 3D structure.

Within the crystallographic *ab* plane, the Co^{II} complexes adopt honeycomb-type layers which assemble in the *c* direction to form helical channels with 6_3 screw symmetry (Figure 1c,d and Figures S2 and S3). The resulting extended supramolecular network is characterized by solvent-accessible voids corresponding to ca. 58% of the unit cell volume (see the Supporting Information). **Hal-MOM-2** is insoluble in H_2O and alcohols; upon reflux in DMF only small quantities dissolve, whereby mass spectra confirm the integrity of the dissolved $[Co_3(\mathbf{L2})_2(H_2O)_6]^{6+}$ species.

The open supramolecular network structure containing hydrated Co^{II} centers prompted us to assess **Hal-MOM-2** as a light-driven heterogeneous H_2O oxidation catalyst in a three-component system using a Clark electrode (Figure 2a). Optimal catalytic performance was observed using **Hal-MOM-2** loadings of between 0.04 and 0.08 mg and 2.0 mg of $[Ru(bpy)_2(deeb)](PF_6)_2$ photosensitizer in phosphate-buffered aqueous solutions (5 mL, 0.01 M, initial pH 7) containing $Na_2S_2O_8$ as a sacrificial two-electron acceptor. Control experiments in which one of each of these three components were removed resulted in negligible O_2 evolution (see the Supporting Information). Upon light irradiation (λ = 470 nm), the dissolved O_2 concentration continuously increases, reaching a plateau at up to 640 μmol/L before leveling off and slowly decreasing after ca. 200 s due to equilibration with the headspace of the reactor.

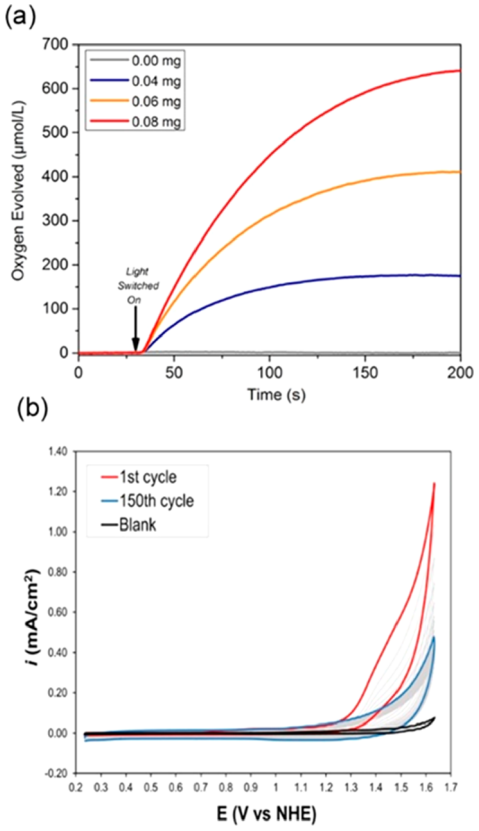

Figure 2. (a) Light-induced H_2O oxidation catalysis at various **Hal-MOM-2** loadings: gray, 0 mg; blue, 0.04 mg (TON = 44; TOF = 1.02 s^{-1}; yield (O_2) = 3.6%); yellow, 0.06 mg (TON = 66; TOF = 1.26 s^{-1}; yield (O_2) = 8.2%); red, 0.08 mg (TON = 78; TOF = 1.09 s^{-1}; yield (O_2) = 12.9%). Conditions: LED (λ = 470, 10 mW cm^{-2}), 2.0 mg of $[Ru(bpy)_2(deeb)](PF_6)_2$, 11.9 mg of $Na_2S_2O_8$ in 5 mL of 0.01 M phosphate buffer (initial pH 7, T = 25 °C). (b) Repetitive CV: red, first scan; blue, last scan after 150 cycles (scan rate = 100 mV/s); black, blank experiment without catalyst.

Under these conditions **Hal-MOM-2** functions as an effective H_2O oxidation catalyst operating with a maximum TON = 78 and reaching an O_2 yield of 12.9% at a catalyst loading of 0.08 mg. The maximum TOF = 1.26 s^{-1} was achieved using a catalytic loading of 0.06 mg. Postcatalytic characterization experiments could not detect *in situ* cobalt oxide (CoO_x) or cobalt phosphate formation or the leaching of Co^{II} ions from **Hal-MOM-2** under the working conditions (Supporting Information).

Recycling tests, involving the addition of photosensitizer and oxidant, demonstrate that **Hal-MOM-2** retains its activity after O_2 evolution; however, the evolved O_2 quantity is reduced in consecutive runs (Figure S20). This reduction can be attributed to a reduction in pH value.

Dissolving the residual material in DMF after three photocatalytic tests and analyzing using ESI-MS revealed that the signal for $\{Co_3\mathbf{L2}_2(H_2O)_5Cl_6\}^+$ at m/z 1669.18 had essentially disappeared, while residual signals corresponding to the amine and aldehyde hydrolysis products remained present at m/z 96.03 and 352.18 (Figures S21 and S22), confirming the hydrolytic disassembly of the supramolecular structure during catalysis.

To further confirm and characterize the photocatalytic O_2 evolution reaction (OER), cyclic voltammetry (CV) experiments were carried out in phosphate buffer at pH 7 using modified carbon-paste electrodes containing 5 wt % catalyst loadings (**Hal-MOM-2**/CP). Figure 2b compares their response during 150 cycles with a control experiment in the absence of **Hal-MOM-2**. The **Hal-MOM-2**/CP electrode clearly exhibits catalytic OER behavior at an onset potential of 1.28 V vs NHE, which corresponds to an onset overpotential of 465 mV. The shoulder at ca. 1.45 V can be attributed to the one-electron Co^{II}/Co^{III} oxidation, which shifts ca. 120 mV to cathodic potentials when the experiment is performed at pH 9 (Figure S23), indicating that the Co^{II}/Co^{III} oxidation proceeds via a proton-coupled electron transfer (PCET) step. Similar to the recycling tests under light-driven conditions, the OER activity decreases within the first 10 cycles; however, it then remains relatively stable for the rest of the experiment. The maintained activity can be attributed to a stabilizing effect of the carbon blend.[32] The electrochemical response confirms that the OER activity under the working conditions is not caused by oxides (CoO_x), as these would result in higher OER activity at lower potentials upon cycling.[40] Such an activity enhancement is indeed observed under highly basic conditions, under which *in situ* CoO_x formation can occur (Figure S23).

Density functional theory (DFT) calculations at the B3LYP level were applied to elucidate the catalytic pathway (Figure 3a, see also the Supporting Information). As the locations of the Co^{II} centers in **Hal-MOM-2** prohibit the direct coupling of two oxo moieties, O−O bond formation was assumed to occur via a water nucleophilic attack (WNA) pathway.[41] Thus, the single-site model $[Co(\mathbf{L2'})_2(H_2O)_2]^{2+}$ was employed, in which **L2** was replaced by (1*H*-imidazol-4-ylmethylenenimine)phenyl

https://dx.doi.org/10.1021/acs.inorgchem.0c02182
Inorg. Chem. XXXX, XXX, XXX−XXX

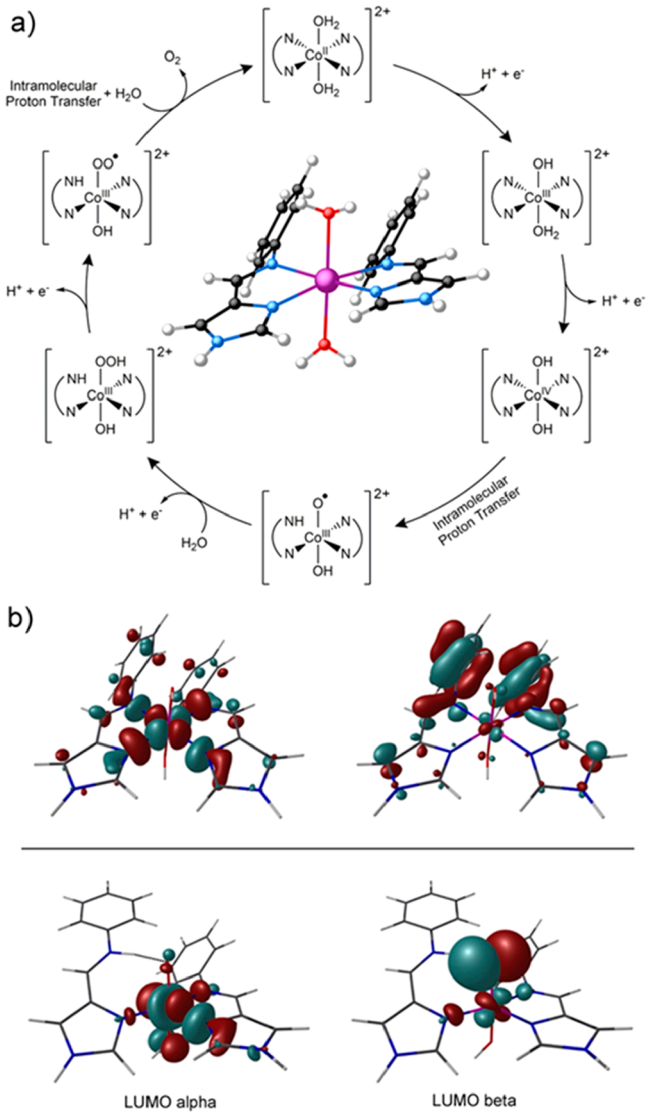

Figure 3. (a) Proposed OER mechanism for $[Co(\mathbf{L2'})_2(H_2O)_2]^{2+}$ on the basis of DFT-B3LYP calculations. Inset: ball and stick representation of $[Co(\mathbf{L2'})_2(H_2O)_2]^{2+}$. (b) LUMOs of the α and β electrons of $[Co^{IV}(\mathbf{L2'})_2(OH)_2]^{2+}$ (top) and $[(NH)Co^{III}(\mathbf{L2'})_2(O^{\bullet})(OH)]^{2+}$ (bottom) species. The LUMO of the β electrons of $[(NH)Co^{III}(\mathbf{L2'})_2(O^{\bullet})(OH)]^{2+}$ is mainly localized on the oxyl radical (right bottom), indicating that this is the active species for accepting the WNA (N∩N = **L2′** = (1*H*-imidazol-4-ylmethylenenimine)-phenyl).

(**L2′**). DFT calculations show that the reaction proceeds via two consecutive PCET steps, in which the two axial H_2O molecules are deprotonated followed by the concomitant two-electron oxidation of the Co^{II} center to form $[Co^{IV}(\mathbf{L2'})_2(OH)_2]^{2+}$. These PCET events are calculated to require 1.64 and 1.67 V (vs NHE, pH 7), respectively, in good agreement with the recorded experimental CV. Nucleophilic H_2O binding followed by PCET generally occurs when a catalyst comprises an oxo group with an unoccupied molecular orbital localized at the O atom, which acts as an electrophile.[41] Thus, for $[Co^{IV}(\mathbf{L2'})_2(OH)_2]^{2+}$, additional deprotonation events are required, as the LUMO shows no contribution of the hydroxyl O atoms (Figure 3b, top). For imines, proton transfer (PT) preferentially occurs intramolecularly, whereby the most basic N atom acts as an H^+ acceptor, yielding $[(NH)Co^{III}(\mathbf{L2'})_2(O^{\bullet})(OH)]^{2+}$, which formally represents a Co^{III}-oxyl radical. The prevalence of Co^{III}-oxyl over Co^{IV}-oxo species has previously been reported for other Co^{II}-based OER catalysts.[42] This intramolecular PT step entails the breaking of the Co−N bond and requires a Gibbs energy of only 0.20 eV (see the Supporting Information for details), whereby the LUMO of the species is mainly localized at the oxyl radical O atom (Figure 3b, bottom). The alternative PT from $[Co^{IV}(\mathbf{L2'})_2(OH)_2]^{2+}$ to the bulk solution demands a Gibbs energy of 1.69 eV, rendering this process highly unlikely. Hence, the reaction is calculated to proceed via a $[(NH)Co^{III}(\mathbf{L2'})_2(O^{\bullet})(OH)]^{2+}$ intermediate, which undergoes nucleophilic attack by a H_2O molecule to form the O−O bond. Subsequent PCET events require 1.29 and 0.56 eV to yield $[(NH)Co^{III}(\mathbf{L2'})_2(OOH)(OH)]^{2+}$ and the superoxide species $[(NH)Co^{III}(\mathbf{L2'})_2(OO^{\bullet})(OH)]^{2+}$, respectively, prior to the release of O_2.

Finally, the initial Co^{II} catalyst is recycled upon H_2O coordination, intramolecular PT, and re-formation of the Co−N bond. This final chemical step is exergonic by −2.16 eV (see the Supporting Information). The DFT-computed mechanism defines the second PCET event as the potential-determining step (PDS). The calculations predict a theoretical overpotential of 853 mV associated with this step, which agrees well with the experimental value of 846 mV to reach 1 mA/cm^2.

The proposed mechanism is in line with the cyclovoltammetry data, which support that the H_2O oxidation is initiated by two consecutive proton-coupled-electron-transfer events. In addition, the observed deactivation pathway under acidic conditions and the mass spectra identifying the ligand hydrolysis products are supportive of the DFT calculations. The single-crystal structure identifies the H_2O binding sites and supports that the O−O bond formation cannot proceed through the interaction with two metal oxo species (I2M) and most likely occurs via water nucleophilic attack.

It is informative to relate the OER activity of **Hal-MOM-2** to those of other reported OER catalysts containing Schiff base ligands. However, direct quantitative comparisons are difficult to establish (see Table S7 in the Supporting Information), considering various working conditions and the heterogeneous nature of our catalyst. In comparison, the selected Ru- and Ir-based catalysts yield very high TONs due to their intrinsic catalytic activities and their higher stability under harsh conditions. However, **Hal-MOM-2** performs favorable kinetics. Examples of OER catalysts containing Schiff base ligands and earth-abundant metal ions are relatively rare.[31] A dimanganese tetrakis-Schiff base macrocycle was reported as an OER catalyst, achieving a TON of 11.2 and a maximum O_2 evolution rate of ca. 15 nmol of O_2 per minute.[43] The heterogeneous electrocatalytic OER activity of two Co-containing, O-phenylenediamine-derived imine complexes, denoted MRC and RSP, was studied, achieving an onset overpotential of 450 mV for RSP in slightly basic, borate-buffered solution.[44] However, the activity of both catalysts decreases upon lowering the pH of the reaction media to neutral values. **Hal-MOM-2** reveals an OER activity comparable to that of RSP. The differences in electrocatalytic activity may partially stem from a lower number of exposed active sites of **Hal-MOM-2** within the CP blend. Moreover, higher pH values increase the OER due to a higher concentration of OH^- ions. The provided comparison, although qualitative, illustrates the good capabilities of **Hal-**

https://dx.doi.org/10.1021/acs.inorgchem.0c02182
Inorg. Chem. XXXX, XXX, XXX−XXX

MOM-2 toward H_2O oxidation and places this catalyst among the best of its kind.

CONCLUSIONS

In conclusion, we report novel {Co^{II}/imine} polygons with tetrahedral and trigonal-disk topologies and demonstrate how supramolecules with hydrated Co^{II} centers can catalyze the highly endergonic H_2O oxidation reaction. The supramolecular 3D network structure of **Hal-MOM-2** promotes both electro- and photocatalytic OER, leading to an onset overpotential of ca. 465 mV and a relatively high TOF_{max} = 1.26 s^{-1}. DFT calculations support the experimental data, attributing the catalytic activity to a Co^{III}-oxyl species, and propose an intermediate Co−N bond cleavage. This possible hydrolytic decomposition pathway is in line with the detection of ligand reactants in the postcatalytic reaction media and might explain the experimentally observed decrease in catalytic activity. Considering that these and other reported supramolecules can form through subcomponent synthesis,[1−3] reversible disassembly/assembly cycles may in the future allow the preparation of catalysts with prolonged activity, hence applying supramolecular concepts to H_2O oxidation catalysts.[45]

EXPERIMENTAL SECTION

Synthesis of $[Co_4(L1)_4]^{8+}$ (1). A slurry of 1,3,5-tris(4-aminophenyl)benzene (120 mg, 0.34 mmol) and 1-methyl-2-imidazolecarboxaldehyde (110 mg, 1.00 mmol) in methanol (20 mL) was stirred for 30 min and then heated at reflux for 2 h, after which time $Co(NO_3)_2{\cdot}6H_2O$ (151 mg, 0.52 mmol) in methanol (10 mL) was added dropwise. The resulting slurry was heated at reflux for a further 4 h, and the precipitate was collected and the filtrate set aside. The solid residue was then washed with ether, dried, and dissolved in DMF. Slow diffusion of THF into this solution afforded single crystals of ([**1**]$(NO_3)_8$·(solv) after 5 days. Yield: 39 mg. Anal. Found: C, 55.5; H, 4.2; N, 18.3. Calcd for $Co_4C_{156}H_{144}N_{44}O_{30}$ ([**1**]$(NO_3)_8{\cdot}6H_2O$): C, 55.9; H, 4.3; N, 18.4. FT-IR (cm^{-1}): 3246 (br), 3082 (w), 2932 (w), 2253 (w), 2595 (w), 1714 (s), 1598 (s), 1514 (m), 1381 (s), 1244 (m), 1139 (m), 1012 (m), 839 (s), 786 (m), 713 (m).

Synthesis of $[Co_3(L2)_2(H_2O)_6]^{6+}$ (2). Ligand **L2** (100 mg, 0.17 mmol) in DMF (7 mL) was treated with $CoCl_2{\cdot}6H_2O$ (60 mg, 0.25 mmol) and then heated at 75 °C for 2 h to give a green solution. This solution was filtered, and slow diffusion of THF into this solution afforded orange crystals of [**2**]Cl_6·(solv) after 24 h. Yield: 50 mg. FT-IR (cm^{-1}); 3365 (m), 1611 (s), 1589 (s), 1497 (s), 1440 (s), 1386 (s), 1324 (m), 1292 (w), 1253 (w), 1173 (w), 1096 (m), 1015 (w), 978 (w), 906 (w), 835 (m), 781 (w), 660 (s). Anal. Found: C, 48.9; H, 5.5; N, 13.0. Calcd for $Co_3C_{75}H_{91}N_{19}O_{16}Cl_6$ ([**2**]Cl_6·DMF·$9H_2O$): C, 48.9; H, 5.2; N, 13.4.

Crystal data and details of data collection and refinement of the compounds are summarized in Table S1 in the Supporting Information. Crystallographic data, CCDC 1867727 and 1867728, can be obtained free of charge from the Cambridge Crystallographic Data Centre via www.ccdc.cam.ac.uk/data_request/cif.

ASSOCIATED CONTENT

Supporting Information

The Supporting Information is available free of charge at https://pubs.acs.org/doi/10.1021/acs.inorgchem.0c02182.

Experimental section and methods, single-crystal X-ray diffraction, additional and enlarged images of **1** and **2**, UV−vis titration analysis, mass spectrometry of the metallo-supramolecular compounds, infrared spectra of the coordination complexes, X-ray powder diffraction, thermogravimetric analysis, light-driven water oxidation measurements, electrochemical analysis of [**2**]Cl_6·DMF·$9H_2O$, DFT calculations, and OER activity comparison with literature examples (PDF)

Accession Codes

CCDC 1867727−1867728 contain the supplementary crystallographic data for this paper. These data can be obtained free of charge via www.ccdc.cam.ac.uk/data_request/cif, or by emailing data_request@ccdc.cam.ac.uk, or by contacting The Cambridge Crystallographic Data Centre, 12 Union Road, Cambridge CB2 1EZ, UK; fax: +44 1223 336033.

AUTHOR INFORMATION

Corresponding Author

Wolfgang Schmitt − *School of Chemistry & AMBER Center, Trinity College, University of Dublin, Dublin D02 PN40, Ireland;* orcid.org/0000-0002-0058-9404; Email: schmittw@tcd.ie

Authors

Ayuk M. Ako − *School of Chemistry & AMBER Center, Trinity College, University of Dublin, Dublin D02 PN40, Ireland*

Amal Cherian Kathalikkattil − *School of Chemistry & AMBER Center, Trinity College, University of Dublin, Dublin D02 PN40, Ireland;* orcid.org/0000-0002-7351-0357

Rory Elliott − *School of Chemistry & AMBER Center, Trinity College, University of Dublin, Dublin D02 PN40, Ireland*

Joaquín Soriano-López − *School of Chemistry & AMBER Center, Trinity College, University of Dublin, Dublin D02 PN40, Ireland;* orcid.org/0000-0002-9203-3752

Ian M. McKeogh − *School of Chemistry & AMBER Center, Trinity College, University of Dublin, Dublin D02 PN40, Ireland*

Muhammad Zubair − *School of Chemistry & AMBER Center, Trinity College, University of Dublin, Dublin D02 PN40, Ireland*

Nianyong Zhu − *School of Chemistry & AMBER Center, Trinity College, University of Dublin, Dublin D02 PN40, Ireland*

Max García-Melchor − *School of Chemistry & AMBER Center, Trinity College, University of Dublin, Dublin D02 PN40, Ireland;* orcid.org/0000-0003-1348-4692

Paul E. Kruger − *MacDiarmid Institute for Advanced Materials and Nanotechnology, School of Physical and Chemical Sciences, University of Canterbury, Christchurch 8041, New Zealand;* orcid.org/0000-0003-4847-6780

Complete contact information is available at: https://pubs.acs.org/10.1021/acs.inorgchem.0c02182

Author Contributions

W.S. conceived the project and performed data analyses. A.M.A., I.M.M., and M.Z. synthesized and characterized the compounds. A.C.K. and R.E. performed the light-induced experiments and characterization. J.S.-L. performed the electrochemical experiments, characterization, and DFT calculations. N.Z. refined the single-crystal X-ray data. M.G.-M. supervised and was involved in the DFT analysis and data interpretation. P.E.K. was involved in data analysis and ligand design. The manuscript was written through contributions of all authors.

Author Contributions

⊥A.M.A., A.C.K., R.E., and J.S.-L. contributed equally.

https://dx.doi.org/10.1021/acs.inorgchem.0c02182
Inorg. Chem. XXXX, XXX, XXX−XXX

Notes

The authors declare no competing financial interest.

■ ACKNOWLEDGMENTS

Funding from the European Research Council (CoG 2014−647719) and Science Foundation Ireland (13/IA/1896) is acknowledged. J.S-L. acknowledges funding from the European Union's Horizon 2020 research and innovation programme under the Marie Skłodowska-Curie grant agreement No 713567. ICHEC and the TCHPC unit are acknowledged for the provision of computational resources.

■ REFERENCES

(1) Yoshizawa, M.; Klosterman, J. K.; Fujita, M. Functional Molecular Flasks: New Properties and Reactions within Discrete, Self-Assembled Hosts. *Angew. Chem., Int. Ed.* **2009**, *48* (19), 3418−3438.

(2) Leininger, S.; Olenyuk, B.; Stang, P. J. Self-Assembly of Discrete Cyclic Nanostructures Mediated by Transition Metals. *Chem. Rev.* **2000**, *100* (3), 853−908.

(3) Zarra, S.; Wood, D. M.; Roberts, D. A.; Nitschke, J. R. Molecular Containers in Complex Chemical Systems. *Chem. Soc. Rev.* **2015**, *44* (2), 419−432.

(4) Brown, C. J.; Toste, F. D.; Bergman, R. G.; Raymond, K. N. Supramolecular Catalysis in Metal−Ligand Cluster Hosts. *Chem. Rev.* **2015**, *115* (9), 3012−3035.

(5) Kaphan, D. M.; Levin, M. D.; Bergman, R. G.; Raymond, K. N.; Toste, F. D. A Supramolecular Microenvironment Strategy for Transition Metal Catalysis. *Science* **2015**, *350* (6265), 1235−1238.

(6) Therrien, B. Drug Delivery by Water-Soluble Organometallic Cages. *Top. Curr. Chem.* **2011**, *319*, 35−55.

(7) Wang, J.; He, C.; Wu, P.; Wang, J.; Duan, C. An Amide-Containing Metal−Organic Tetrahedron Responding to a Spin-Trapping Reaction in a Fluorescent Enhancement Manner for Biological Imaging of NO in Living Cells. *J. Am. Chem. Soc.* **2011**, *133* (32), 12402−12405.

(8) Ward, M. D.; Raithby, P. R. Functional Behaviour from Controlled Self-Assembly: Challenges and Prospects. *Chem. Soc. Rev.* **2013**, *42* (4), 1619−1636.

(9) Yan, X.; Cook, T. R.; Wang, P.; Huang, F.; Stang, P. J. Highly Emissive Platinum(II) Metallacages. *Nat. Chem.* **2015**, *7* (4), 342−348.

(10) Sanz, S.; O'Connor, H. M.; Pineda, E. M.; Pedersen, K. S.; Nichol, G. S.; Mønsted, O.; Weihe, H.; Piligkos, S.; McInnes, E. J. L.; Lusby, P. J.; Brechin, E. K. $[Cr^{III}8M^{II}6]^{12+}$ Coordination Cubes (M^{II} = Cu, Co). *Angew. Chem., Int. Ed.* **2015**, *54* (23), 6761−6764.

(11) Luo, D.; Zhou, X.-P.; Li, D. Beyond Molecules: Mesoporous Supramolecular Frameworks Self-Assembled from Coordination Cages and Inorganic Anions. *Angew. Chem., Int. Ed.* **2015**, *54* (21), 6190−6195.

(12) Breen, J. M.; Schmitt, W. Hybrid Organic-Inorganic Polyoxometalates: Functionalization of V^{IV}/V^{V} Nanosized Clusters to Produce Molecular Capsules. *Angew. Chem., Int. Ed.* **2008**, *47* (36), 6904−6908.

(13) Rizzuto, F. J.; Wu, W.-Y.; Ronson, T. K.; Nitschke, J. R. Peripheral Templation Generates an $M^{II}_6L_4$ Guest-Binding Capsule. *Angew. Chem., Int. Ed.* **2016**, *55* (28), 7958−7962.

(14) Tranchemontagne, D. J.; Ni, Z.; O'Keeffe, M.; Yaghi, O. M. Reticular Chemistry of Metal−Organic Polyhedra. *Angew. Chem., Int. Ed.* **2008**, *47* (28), 5136−5147.

(15) Byrne, K.; Zubair, M.; Zhu, N.; Zhou, X.-P.; Fox, D. S.; Zhang, H.; Twamley, B.; Lennox, M. J.; Düren, T.; Schmitt, W. Ultra-Large Supramolecular Coordination Cages Composed of Endohedral Archimedean and Platonic Bodies. *Nat. Commun.* **2017**, *8*, 15268.

(16) Jiménez, A.; Bilbeisi, R. A.; Ronson, T. K.; Zarra, S.; Woodhead, C.; Nitschke, J. R. Selective Encapsulation and Sequential Release of Guests Within a Self-Sorting Mixture of Three Tetrahedral Cages. *Angew. Chem., Int. Ed.* **2014**, *53* (18), 4556−4560.

(17) Xu, W.-Q.; Li, Y.-H.; Wang, H.-P.; Jiang, J.-J.; Fenske, D.; Su, C.-Y. Face-Capped M_4L_4 Tetrahedral Metal-Organic Cage: Iodine Capture and Release, Ion Exchange, and Electrical Conductivity. *Chem. - Asian J.* **2016**, *11* (2), 216−220.

(18) Xu, W.-Q.; Fan, Y.-Z.; Wang, H.-P.; Teng, J.; Li, Y.-H.; Chen, C.-X.; Fenske, D.; Jiang, J.-J.; Su, C.-Y. Investigation of Binding Behavior between Drug Molecule 5-Fluoracil and M_4L_4-Type Tetrahedral Cages: Selectivity, Capture, and Release. *Chem. - Eur. J.* **2017**, *23* (15), 3542−3547.

(19) Zhang, D.; Ronson, T. K.; Mosquera, J.; Martinez, A.; Nitschke, J. R. Selective Anion Extraction and Recovery Using a $Fe^{II}_4L_4$ Cage. *Angew. Chem., Int. Ed.* **2018**, *57* (14), 3717−3721.

(20) Biros, S. M.; Yeh, R. M.; Raymond, K. N. Design and Formation of a Large Tetrahedral Cluster Using 1,1′-Binaphthyl Ligands. *Angew. Chem., Int. Ed.* **2008**, *47* (32), 6062−6064.

(21) McConnell, A. J.; Aitchison, C. M.; Grommet, A. B.; Nitschke, J. R. Subcomponent Exchange Transforms an $Fe^{II}_4L_4$ Cage from High- to Low-Spin, Switching Guest Release in a Two-Cage System. *J. Am. Chem. Soc.* **2017**, *139* (18), 6294−6297.

(22) Tidmarsh, I. S.; Taylor, B. F.; Hardie, M. J.; Russo, L.; Clegg, W.; Ward, M. D. Further Investigations into Tetrahedral M_4L_6 Cage Complexes Containing Guest Anions: New Structures and NMR Spectroscopic Studies. *New J. Chem.* **2009**, *33* (2), 366−375.

(23) Fujita, D.; Ueda, Y.; Sato, S.; Mizuno, N.; Kumasaka, T.; Fujita, M. Self-Assembly of Tetravalent Goldberg Polyhedra from 144 Small Components. *Nature* **2016**, *540* (7634), 563−566.

(24) Ferguson, A.; Squire, M. A.; Siretanu, D.; Mitcov, D.; Mathonière, C.; Clérac, R.; Kruger, P. E. A Face-Capped $[Fe_4L_4]^{8+}$ Spin Crossover Tetrahedral Cage. *Chem. Commun.* **2013**, *49* (16), 1597.

(25) Bilbeisi, R. A.; Clegg, J. K.; Elgrishi, N.; Hatten de, X.; Devillard, M.; Breiner, B.; Mal, P.; Nitschke, J. R. Subcomponent Self-Assembly and Guest-Binding Properties of Face-Capped $Fe_4L_4^{8+}$ Capsules. *J. Am. Chem. Soc.* **2012**, *134* (11), 5110−5119.

(26) Riddell, I. A.; Hristova, Y. R.; Clegg, J. K.; Wood, C. S.; Breiner, B.; Nitschke, J. R. Five Discrete Multinuclear Metal-Organic Assemblies from One Ligand: Deciphering the Effects of Different Templates. *J. Am. Chem. Soc.* **2013**, *135* (7), 2723−2733.

(27) Lewis, N. S.; Nocera, D. G. Powering the Planet: Chemical Challenges in Solar Energy Utilization. *Proc. Natl. Acad. Sci. U. S. A.* **2006**, *103* (43), 15729−15735.

(28) Suen, N.-T.; Hung, S.-F.; Quan, Q.; Zhang, N.; Xu, Y.-J.; Chen, H. M. Electrocatalysis for the Oxygen Evolution Reaction: Recent Development and Future Perspectives. *Chem. Soc. Rev.* **2017**, *46* (2), 337−365.

(29) Blakemore, J. D.; Crabtree, R. H.; Brudvig, G. W. Molecular Catalysts for Water Oxidation. *Chem. Rev.* **2015**, *115* (23), 12974−13005.

(30) McCrory, C. C. L.; Jung, S.; Ferrer, I. M.; Chatman, S. M.; Peters, J. C.; Jaramillo, T. F. Benchmarking Hydrogen Evolving Reaction and Oxygen Evolving Reaction Electrocatalysts for Solar Water Splitting Devices. *J. Am. Chem. Soc.* **2015**, *137* (13), 4347−4357.

(31) Kärkäs, M. D.; Åkermark, B. Water Oxidation Using Earth-Abundant Transition Metal Catalysts: Opportunities and Challenges. *Dalt. Trans.* **2016**, *45* (37), 14421−14461.

(32) Blasco-Ahicart, M.; Soriano-López, J.; Carbó, J. J.; Poblet, J. M.; Galan-Mascaros, J. R. Polyoxometalate Electrocatalysts Based on Earth-Abundant Metals for Efficient Water Oxidation in Acidic Media. *Nat. Chem.* **2018**, *10* (1), 24−30.

(33) Barnett, S. M.; Goldberg, K. I.; Mayer, J. M. A Soluble Copper−Bipyridine Water-Oxidation Electrocatalyst. *Nat. Chem.* **2012**, *4* (6), 498−502.

(34) Panda, C.; Debgupta, J.; Díaz Díaz, D.; Singh, K. K.; Sen Gupta, S.; Dhar, B. B. Homogeneous Photochemical Water Oxidation by Biuret-Modified Fe-TAML: Evidence of $Fe^{V}(O)$ Intermediate. *J. Am. Chem. Soc.* **2014**, *136* (35), 12273−12282.

(35) An, Y.; Liu, Y.; An, P.; Dong, J.; Xu, B.; Dai, Y.; Qin, X.; Zhang, X.; Whangbo, M.-H.; Huang, B. Ni^{II} Coordination to an Al-Based

https://dx.doi.org/10.1021/acs.inorgchem.0c02182
Inorg. Chem. XXXX, XXX, XXX−XXX

526 Metal-Organic Framework Made from 2-Aminoterephthalate for
527 Photocatalytic Overall Water Splitting. *Angew. Chem., Int. Ed.* **2017**,
528 *56* (11), 3036−3040.
529 (36) Ng, J. W. D.; García-Melchor, M.; Bajdich, M.; Chakthranont,
530 P.; Kirk, C.; Vojvodic, A.; Jaramillo, T. F. Gold-Supported Cerium-
531 Doped NiO_x Catalysts for Water Oxidation. *Nat. Energy* **2016**, *1* (5),
532 16053.
533 (37) Zhang, B.; Zheng, X.; Voznyy, O.; Comin, R.; Bajdich, M.;
534 Garcia-Melchor, M.; Han, L.; Xu, J.; Liu, M.; Zheng, L.; Garcia de
535 Arquer, F. P.; Dinh, C. T.; Fan, F.; Yuan, M.; Yassitepe, E.; Chen, N.;
536 Regier, T.; Liu, P.; Li, Y.; De Luna, P.; Janmohamed, A.; Xin, H. L.;
537 Yang, H.; Vojvodic, A.; Sargent, E. H. Homogeneously Dispersed
538 Multimetal Oxygen-Evolving Catalysts. *Science* **2016**, *352* (6283),
539 333−337.
540 (38) Steiner, T. Hydrogen-Bond Distances to Halide Ions in
541 Organic and Organometallic Crystal Structures: Up-to-date Database
542 Study. *Acta Crystallogr., Sect. B: Struct. Sci.* **1998**, *B54*, 456−463.
543 (39) Liu, Y.; Zhao, W.; Chen, C.-H.; Flood, A. H. Chloride capture
544 using a C−H hydrogen-bonding cage. *Science* **2019**, *365*, 159−161.
545 (40) Deng, X.; Tüysüz, H. Cobalt-Oxide-Based Materials as Water
546 Oxidation Catalyst: Recent Progress and Challenges. *ACS Catal.*
547 **2014**, *4* (10), 3701−3714.
548 (41) Soriano-López, J.; Schmitt, W.; García-Melchor, M. Computa-
549 tional Modelling of Water Oxidation Catalysts. *Curr. Opin. Electro-*
550 *chem.* **2018**, *7*, 22−30.
551 (42) Soriano-López, J.; Musaev, D. G.; Hill, C. L.; Galán-Mascarós,
552 J. R.; Carbó, J. J.; Poblet, J. M. Tetracobalt-Polyoxometalate Catalysts
553 for Water Oxidation: Key Mechanistic Details. *J. Catal.* **2017**, *350*,
554 56−63.
555 (43) Kal, S.; Ayensu-Mensah, L.; Dinolfo, P. H. Evidence for
556 catalytic water oxidation by a dimanganese tetrakis-Schiff base
557 macrocycle. *Inorg. Chim. Acta* **2014**, *423*, 201−206.
558 (44) Huang, B.; Wang, Y.; Zhan, S.; Ye, J. One-step electrochemical
559 deposition of Schiff base cobalt complex as effective water oxidation
560 catalyst. *Appl. Surf. Sci.* **2017**, *396*, 121−128.
561 (45) Costentin, C.; Nocera, D. G. Self-Healing Catalysis in Water.
562 *Proc. Natl. Acad. Sci. U. S. A.* **2017**, *114* (51), 13380−13384.

https://dx.doi.org/10.1021/acs.inorgchem.0c02182
Inorg. Chem. XXXX, XXX, XXX−XXX